Supporting Information for

Dioxygen-Initiated Oxidation of Heteroatomic Substrates Incorporated into Ancillary Pyridine Ligands of Carboxylate-Rich Diiron(II) Complexes

*Emily C. Carson and Stephen J. Lippard**

Department of Chemistry, Massachusetts Institute of Technology, Cambridge, Massachusetts 02139

lippard@mit.edu

RECEIVED DATE August 00, 2005

Table S1. Summary of X-ray Crystallographic Data.

	3·$C_2H_4Cl_2$	**4**·1.5$C_2H_4Cl_2$/C_5H_{12}	**5**·C_6H_5Cl
Empirical Formula	$Fe_2C_{95}H_{62}NO_8F_8PCl_2$	$Fe_2C_{98}H_{93}NO_8SCl_3$	$Fe_2C_{108}H_{92}N_2O_{10}S_2Cl_2$
Formula Weight	1711.03	1662.84	1824.56
Space Group	$P\bar{1}$	$P2_1/c$	$P\bar{1}$
a, Å	13.6676(14)	13.0032(6)	12.3481(13)
b, Å	14.0155(14)	26.3878(12)	13.2842(13)
c, Å	21.278(2)	24.6935(12)	14.8486(16)
α, deg	80.799(2)		107.009(2)
β, deg	89.079(2)	95.8440(10)	103.260(2)
γ, deg	86.533(2)		95.274(3)
V, $Å^3$	4016.0(7)	8428.9(7)	2233.7(4)
Z	2	4	1
ρ_{calc}, g/cm^3	1.415	1.310	1.356
T, ºC	-100	-100	-100
μ(Mo Kα), mm^{-1}	0.526	0.523	0.495
θ limits, deg	1.47 – 26.73	1.66 – 27.10	1.63 – 26.02
total no. of data	33796	72962	18030
no. of unique data	16744	18576	8699
no. of params	1099	1279	572
Goodness-of-fit on F^2	1.030	1.196	0.769
R1[a]	0.0709	0.0786	0.0744
wR^{2}[b]	0.1767	0.1679	0.0999
max, min peaks, $e/Å^3$	1.124, -1.036	1.031, -0.610	0.463, -0.323

[a] $R1 = \Sigma||F_o|-F_c||/\Sigma|F_o|$. [b] $wR^2 = \{\Sigma[w(F_o^2-F_c^2)^2]/\Sigma[w(F_o^2)^2]\}^{1/2}$.

Table S1. Continued.

	6	**7**·4CH_2Cl_2	**8**·3CH_2Cl_2
Empirical Formula	$FeC_{52}H_{44}N_2O_4S_2$	$Fe_6C_{122}H_{110}N_2O_{18}P_2Cl_{12}$	$Fe_2C_{96}H_{68}NO_{12}F_8PCl_6$
Formula Weight	880.86	2714.56	1934.88
Space Group	$P2_1/c$	$P\bar{1}$	$P\bar{1}$
a, Å	18.821(19)	14.508(2)	12.9063(17)
b, Å	12.262(12)	15.852(2)	14.1811(18)
c, Å	21.18(2)	15.904(3)	24.990(3)
α, deg		78.407(3)	78.235(3)
β, deg	115.123(16)	77.951(3)	86.110(2)
γ, deg		63.832(3)	86.837(3)
V, $Å^3$	4425(8)	4042(9)	4463.4(10)
Z	4	1	2
ρ_{calc}, g/cm^3	1.322	1.415	1.440
T, ºC	-100	-100	-100
μ(Mo Kα), mm^{-1}	0.483	1.004	0.602
θ limits, deg	1.95 – 27.16	1.64 – 25.00	1.67 – 27.10
total no. of data	37528	23654	39033
no. of unique data	9779	11127	19334
no. of params	550	730	1151
Goodness-of-fit on F^2	1.131	0.997	0.997
R1[a]	0.0566	0.1032	0.0855
wR^{2}[b]	0.1240	0.1826	0.1521
max, min peaks, $e/Å^3$	0.505, -0.278	1.028, -0.551	0.779, -0.721

[a] $R1 = \Sigma||F_o|-F_c||/\Sigma|F_o|$. [b] $wR^2 = \{\Sigma[w(F_o^2-F_c^2)^2]/\Sigma[w(F_o^2)^2]\}^{1/2}$.

Table S2. Selected Interbond Lengths and Angles for $[Fe_2(\mu\text{-}O_2CAr^{Tol})_2(O_2CAr^{Tol})_2\text{-}(2\text{-}MeS(O)py)_2]$ (**5**)[a]

	Bond Length (Å)		Bond Angle (deg)
Fe1···Fe2	4.586(2)	O1–Fe1–N1	79.1(3)
Fe1–N1	2.156(6)	O2–Fe1–N1	96.7(2)
Fe1–O1	2.234(5)	O3–Fe1–N1	92.4(2)
Fe1–O2	1.961(5)	O4–Fe1–N1	83.62(18)
Fe1–O3	2.071(5)	O5–Fe1–N1	149.98(19)
Fe1–O4	2.160(5)	O1–Fe1–O2	82.09(19)
Fe1–O5	2.267(5)	O1–Fe1–O3	171.5(2)
		O1–Fe1–O4	83.7(2)
		O1–Fe1–O5	97.75(17)
		O2–Fe1–O3	98.6(2)
		O2–Fe1–O4	163.3(2)
		O2–Fe1–O5	112.7(2)
		O3–Fe1–O4	96.08(18)
		O3–Fe1–O5	89.31(17)
		O4–Fe1–O5	59.28(17)

[a]Numbers in parentheses are estimated standard deviations of the last significant figure. Atoms are labeled as indicated Figures 1 and S3.

Table S3. Selected Interbond Distances and Angles for $[Fe(O_2CAr^{Tol})_2(2\text{-HSpy})_2]$ (**6**)[a]

	Bond Length (Å)		Bond Angle (deg)
Fe1–O1	2.052(2)	O1–Fe1–S1	102.69(8)
Fe1–O3	2.029(3)	O1–Fe1–S2	110.22(6)
Fe1–S1	2.398(2)	O3–Fe1–S1	112.35(5)
Fe1–S2	2.398(3)	O3–Fe1–S2	98.59(6)
N1–C1	1.348(3)	O1–Fe1–O3	133.35(9)
C1–C2	1.407(4)	S1–Fe1–S2	92.04(2)
C2–C3	1.367(4)	Fe1–S1–C6	108.93(9)
C3–C4	1.393(4)	Fe1–S2–C6	106.95(9)
C4–C5	1.355(4)		
C5–N1	1.353(4)		
S1–C1	1.716(3)		
N2–C6	1.346(3)		
C6–C7	1.412(4)		
C7–C8	1.363(4)		
C8–C9	1.394(4)		
C9–C10	1.364(4)		
C10–N2	1.346(3)		
S2–C6	1.717(3)		
N1···O4	2.747(3)		
N2···O2	2.706(3)		

[a]Numbers in parentheses are estimated standard deviations of the last significant figure. Atoms are labeled as indicated Figures 1 and S4.

Table S4. Selected Interatomic Distances (Å) and Angles (deg) for $[Fe_6(\mu_4\text{-}O)_2(\mu\text{-}OH)_6(\mu\text{-}O_2CAr^{Tol})_4Cl_4(2\text{-}Ph_2P(O)py)_2]$ (**7**)[a]

Fe1–O1	2.010(7)	Fe2–O3	1.993(6)	Fe3–O2	1.890(7)
Fe1–O2	2.036(6)	Fe2–O3A	1.990(6)	Fe3–O3	2.260(6)
Fe1–O3	1.911(6)	Fe2–O6	2.036(6)	Fe3–O7A	1.922(6)
Fe1–O4	2.049(6)	Fe2–O7	2.022(6)	Fe3–O9	1.898(6)
Fe1–O5	2.044(6)	Fe2–O8	2.007(6)	Fe3–Cl2	2.215(3)
Fe1–Cl1	2.290(3)	Fe2–O9	2.007(6)	Fe3···Fe2	3.143(2)
Fe1–Fe3	3.157(2)	Fe2···Fe2A	3.029(3)	Fe3A···Fe2	3.158(2)
O1–Fe1–Cl1	95.8(2)	O3–Fe2–O3A	81.0(3)	Cl2–Fe3–O2	104.9(2)
O2–Fe1–Cl1	176.8(2)	O3–Fe2–O6	98.5(3)	Cl2–Fe3–O3	177.57(19)
O3–Fe1–Cl1	97.0(2)	O3–Fe2–O7	101.6(3)	Cl2–Fe3–O7A	101.9(2)
O4–Fe1–Cl1	91.7(2)	O3–Fe2–O8	164.8(3)	Cl2–Fe3–O9	105.9(2)
O5–Fe1–Cl1	89.4(2)	O3–Fe2–O9	80.5(3)	O2–Fe3–O3	74.9(2)
O1–Fe1–O2	87.1(3)	O6–Fe2–O3A	164.3(3)	O2–Fe3–O7A	117.2(3)
O1–Fe1–O3	167.1(3)	O6–Fe2–O7	84.2(3)	O2–Fe3–O9	115.5(3)
O1–Fe1–O4	84.9(3)	O6–Fe2–O8	87.6(3)	O3–Fe3–O7A	76.2(2)
O1–Fe1–O5	84.3(3)	O6–Fe2–O9	93.9(3)	O3–Fe3–O9	76.3(2)
O2–Fe1–O3	80.0(3)	O7–Fe2–O3A	80.6(3)	O9–Fe3–O7A	109.7(3)
O2–Fe1–O4	89.8(3)	O7–Fe2–O8	92.7(3)		
O2–Fe1–O5	89.7(3)	O7–Fe2–O9	177.3(3)		
O3–Fe1–O4	95.2(3)	O8–Fe2–O3A	96.893)		
O3–Fe1–O5	95.2(3)	O8–Fe2–O9	85.3(3)		
O4–Fe1–O5	169.3(3)	O9–Fe2–O3A	101.5(3)		

[a]Numbers in parentheses are estimated standard deviations of the last significant figure. Atoms are labeled as indicated Figures 2 and S5.

Table S5. Bond Valence Sum Analysis of Iron-Ligand Bonds in **7** and **8**

Bond	Bond Length (Å)	Bond Valence	Bond Valence Sum
$[Fe_6(\mu_4\text{-}O)_2(\mu\text{-}OH)_6(\mu\text{-}O_2CAr^{Tol})_4Cl_4(2\text{-}Ph_2P(O)py)_2]$ (**7**)			
Fe1–O1	2.010(7)	0.507	3.306
Fe1–O2	2.036(6)	0.473	
Fe1–O3	1.911(6)	0.663	
Fe1–O4	2.049(6)	0.457	
Fe1–O5	2.044(6)	0.463	
Fe1–Cl1	2.290(3)	0.743	
Fe2–O3	1.993(6)	0.531	3.054
Fe2–O3A	1.990(6)	0.536	
Fe2–O6	2.036(6)	0.473	
Fe2–O7	2.022(6)	0.491	
Fe2–O8	2.007(6)	0.512	
Fe2–O9	2.007(6)	0.512	
Fe3–O2	1.890(7)	0.702	3.20
Fe3–O3	2.260(6)	0.258	
Fe3–O7A	1.922(6)	0.644	
Fe3–O9	1.898(6)	0.687	
Fe3–Cl2	2.215(3)	0.910	
$[Fe_2(\mu\text{-}OH)_2(\mu\text{-}O_2CAr^{4\text{-}FPh})(O_2CAr^{4\text{-}FPh})_3(OH_2)(2\text{-}Ph_2P(O)py)]$ (**8**)			
Fe1–N1	2.210(4)	0.383	3.131
Fe1–O1	2.023(3)	0.490	
Fe1–O2	1.954(4)	0.590	
Fe1–O3	1.981(4)	0.549	
Fe1–O5	2.003(3)	0.517	
Fe1–O7	1.947(3)	0.602	
Fe2–O2	1.981(4)	0.549	3.118
Fe2–O3	1.977(4)	0.555	
Fe2–O4	2.097(4)	0.401	
Fe2–O6	2.017(3)	0.498	
Fe2–O9	1.974(3)	0.559	
Fe2–O11	1.976(3)	0.556	

Chart S1

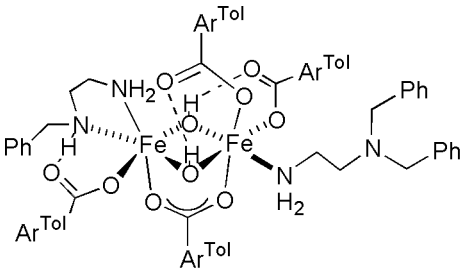
Ar^Tol
NH2
Ph
N
H
Fe
Fe
O
H
N
H2
Ph
Ar^Tol
Ar^Tol
Ar^Tol

9

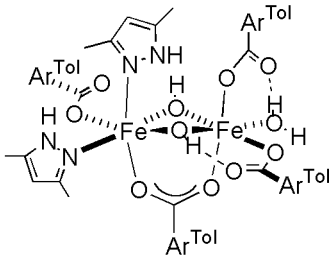
Ar^Tol
N-NH
Ar^Tol
H
O
Fe
Fe
H
O
N
N
Ar^Tol
Ar^Tol

10

Scheme S1

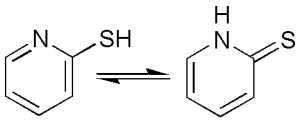

Captions for Supporting Figures

Figure S1. Top: ORTEP diagram of $[Fe_2(\mu\text{-}O_2CAr^{4\text{-}FPh})_3(O_2CAr^{4\text{-}FPh})(2\text{-}Ph_2Ppy)]$ (**3**) illustrating 50% probability thermal ellipsoids for all non-hydrogen atoms. Bottom: Drawing in which the aromatic rings of the $^{-}O_2CAr^{4\text{-}FPh}$ ligands are omitted for clarity.

Figure S2. Top: ORTEP diagram of $[Fe_2(\mu\text{-}O_2CAr^{Tol})_3(O_2CAr^{Tol})(2\text{-}MeSpy)]$ (**4**) showing 50% probability thermal ellipsoids for all non-hydrogen atoms. Bottom: Drawing in which the aromatic rings of $^{-}O_2CAr^{Tol}$ are omitted for clarity.

Figure S3. Top: ORTEP diagram of $[Fe_2(\mu\text{-}O_2CAr^{Tol})_2(O_2CAr^{Tol})_2(2\text{-}MeS(O)py)_2]$ (**5**) showing 50 % probability thermal ellipsoids for all non-hydrogen atoms. Bottom: Drawing in which the aromatic rings of $^{-}O_2CAr^{Tol}$ are omitted for clarity.

Figure S4. Top: ORTEP diagram of $[Fe(O_2CAr^{Tol})_2(2\text{-}HSpy)_2]$ (**6**) showing 50 % probability thermal ellipsoids for all non-hydrogen atoms. Bottom: Drawing in which the aromatic rings of $^{-}O_2CAr^{Tol}$ are omitted for clarity.

Figure S5. Top: ORTEP diagram of $[Fe_6(\mu_4\text{-}O)_2(\mu\text{-}OH)_6(\mu\text{-}O_2CAr^{Tol})_4Cl_4(2\text{-}Ph_2P(O)py)_2]$ (**7**) illustrating 50% probability thermal ellipsoids for all non-hydrogen atoms. Bottom: Drawing in which the aromatic rings of the $^{-}O_2CAr^{Tol}$ ligands are omitted for clarity.

Figure S6. Top: ORTEP diagram of $[Fe_2(\mu\text{-}OH)_2(\mu\text{-}O_2CAr^{4\text{-}FPh})(O_2CAr^{4\text{-}FPh})_3(OH_2)\text{-}(2\text{-}Ph_2P(O)py)]$ (**8**) illustrating 50% probability thermal ellipsoids for all non-hydrogen atoms. Bottom: Drawing in which the aromatic rings of the $^{-}O_2CAr^{4\text{-}FPh}$ ligands are omitted for clarity.

Figure S7. FT-IR spectra of KBr pellets of $[Fe_2(\mu\text{-}O_2CAr^{4\text{-}FPh})_3(O_2CAr^{4\text{-}FPh})(2\text{-}Ph_2Ppy)]$ (**3**) (top) and $[Fe_2(\mu\text{-}OH)_2(\mu\text{-}O_2CAr^{4\text{-}FPh})(O_2CAr^{4\text{-}FPh})_3(OH_2)(2\text{-}Ph_2P(O)py)]$ (**8**) (bottom).

Figure S8. FT-IR spectra of KBr pellets of $[Fe_2(\mu\text{-}O_2CAr^{Tol})_3(O_2CAr^{Tol})(2\text{-}MeSpy)$ (**4**) (top) and $[Fe_2(\mu\text{-}O_2CAr^{Tol})_2(O_2CAr^{Tol})_2(2\text{-}MeS(O)py)_2]$ (**5**) (bottom). The arrow designates ν_{S_O}.

Figure S9. FT-IR spectrum of a KBr pellet of $[Fe(O_2CAr^{Tol})_2(2\text{-}HSpy)_2]$ (**6**).

Figure S10. Mössbauer spectrum (experimental data (|), calculated fit (–)) recorded at 4.2 K for a solid sample of $[Fe_2(\mu\text{-}O_2CAr^{4\text{-}FPh})_3(O_2CAr^{4\text{-}FPh})(2\text{-}Ph_2Ppy)]$ (**3**)).

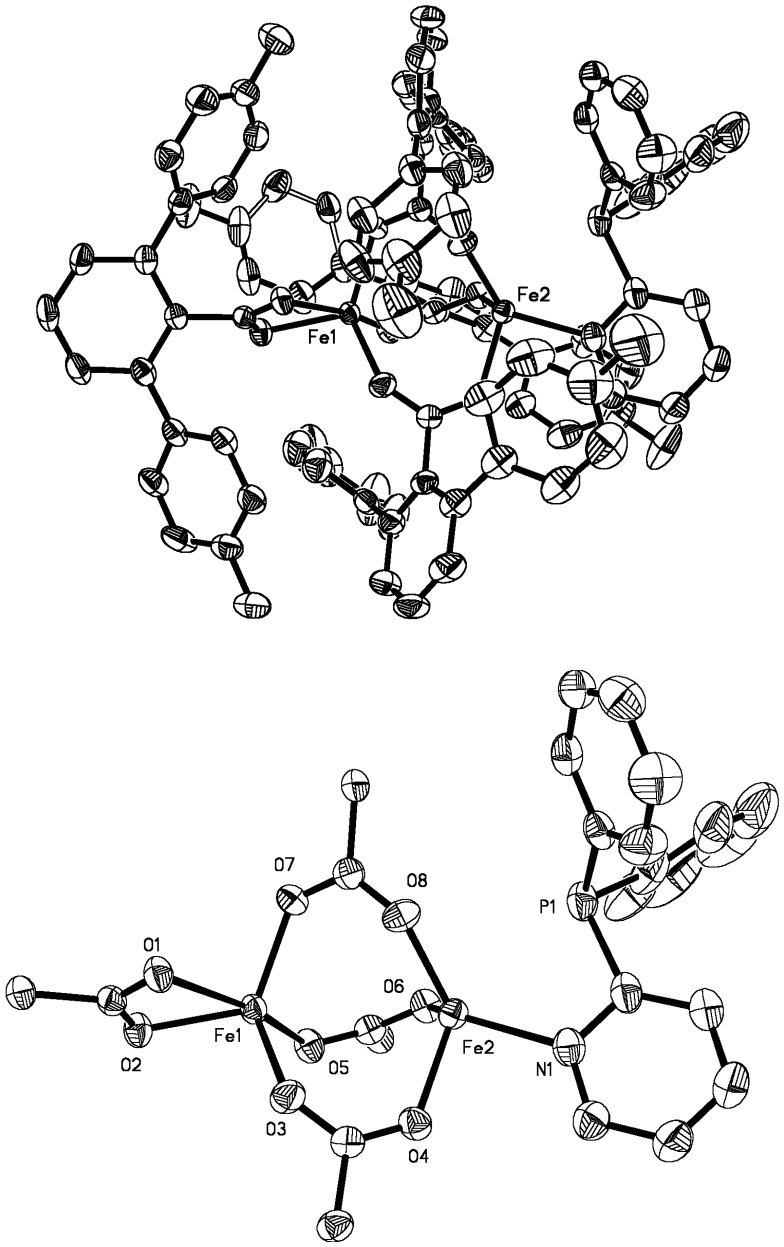

Figure S1. Carson and Lippard

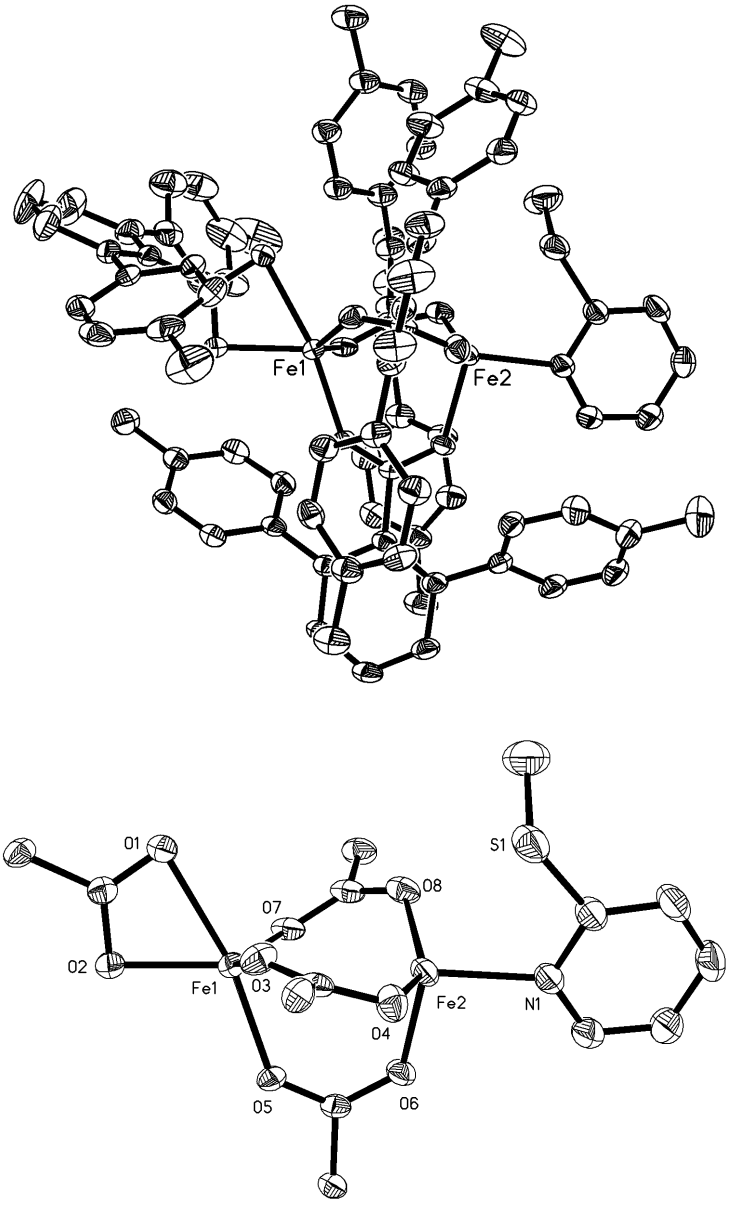

Figure S2. Carson and Lippard

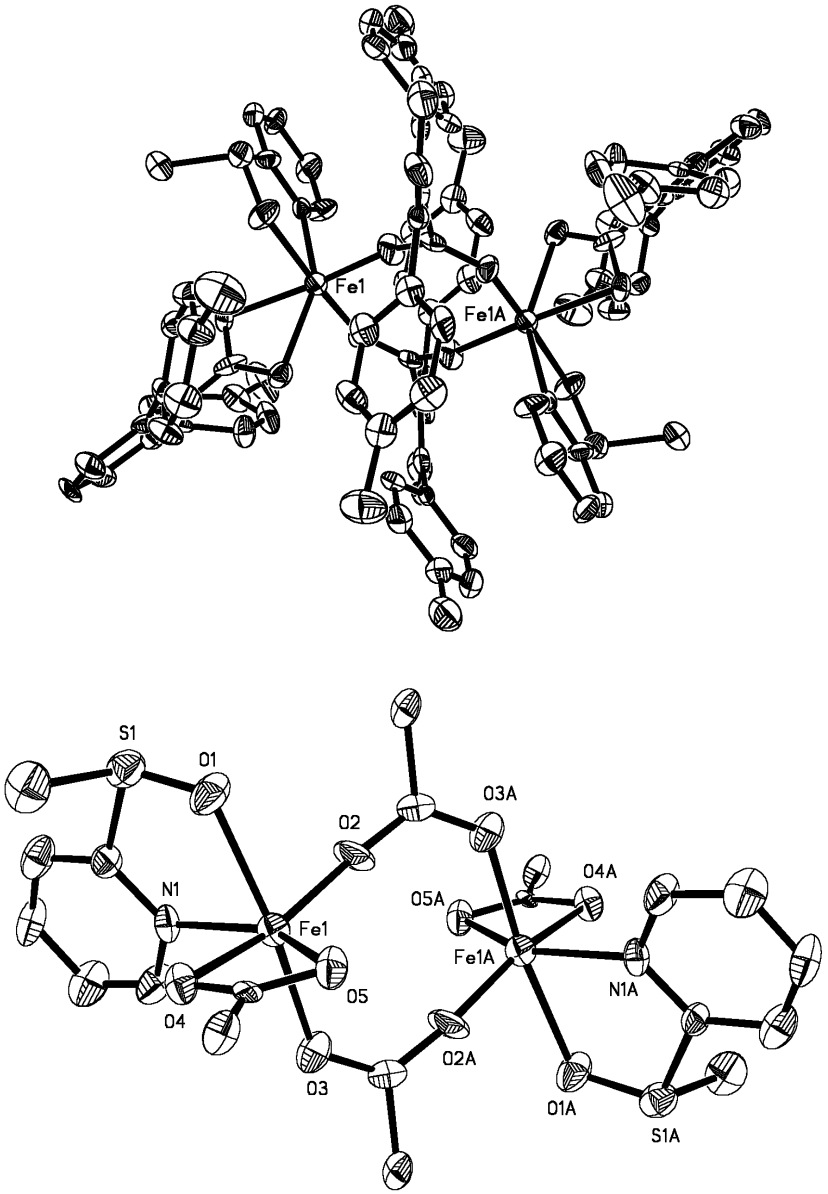

Figure S3. Carson and Lippard

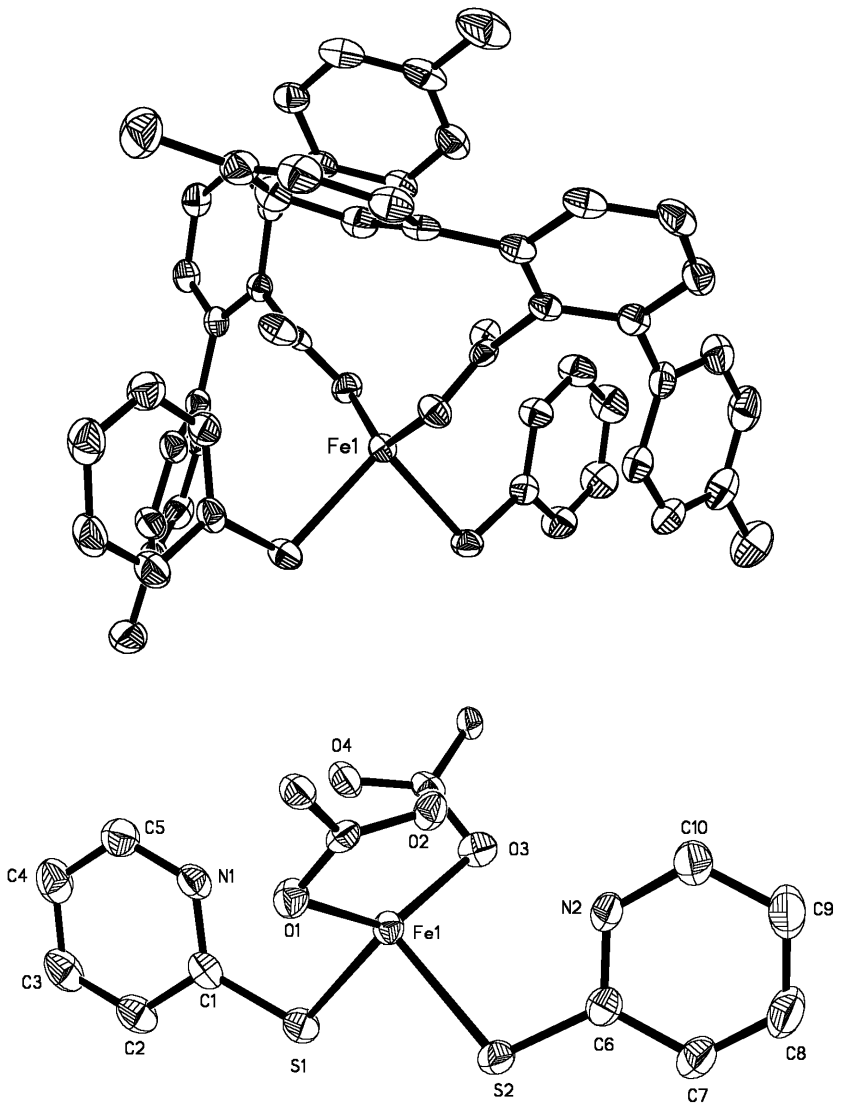

Figure S4. Carson and Lippard

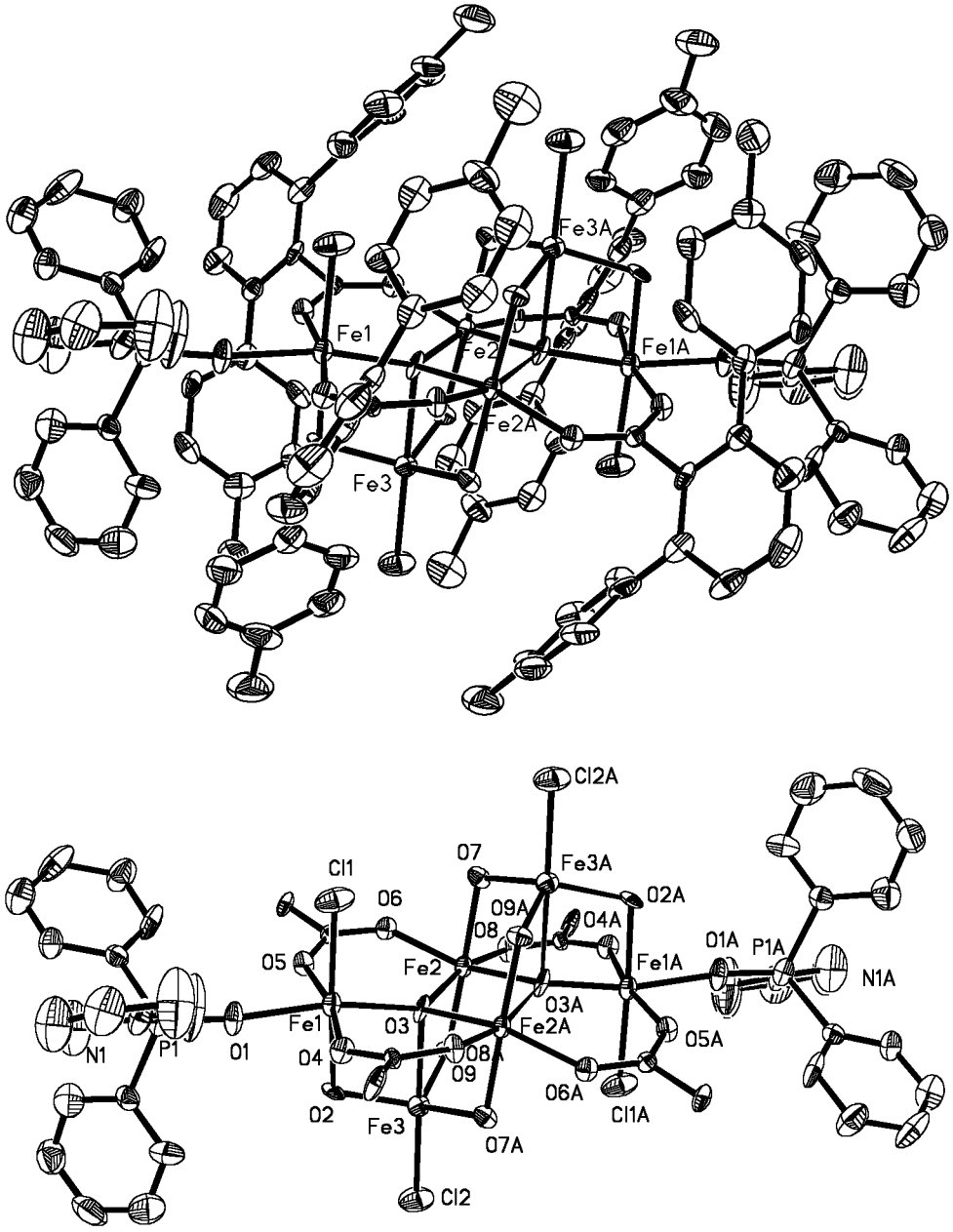

Figure S5. Carson and Lippard

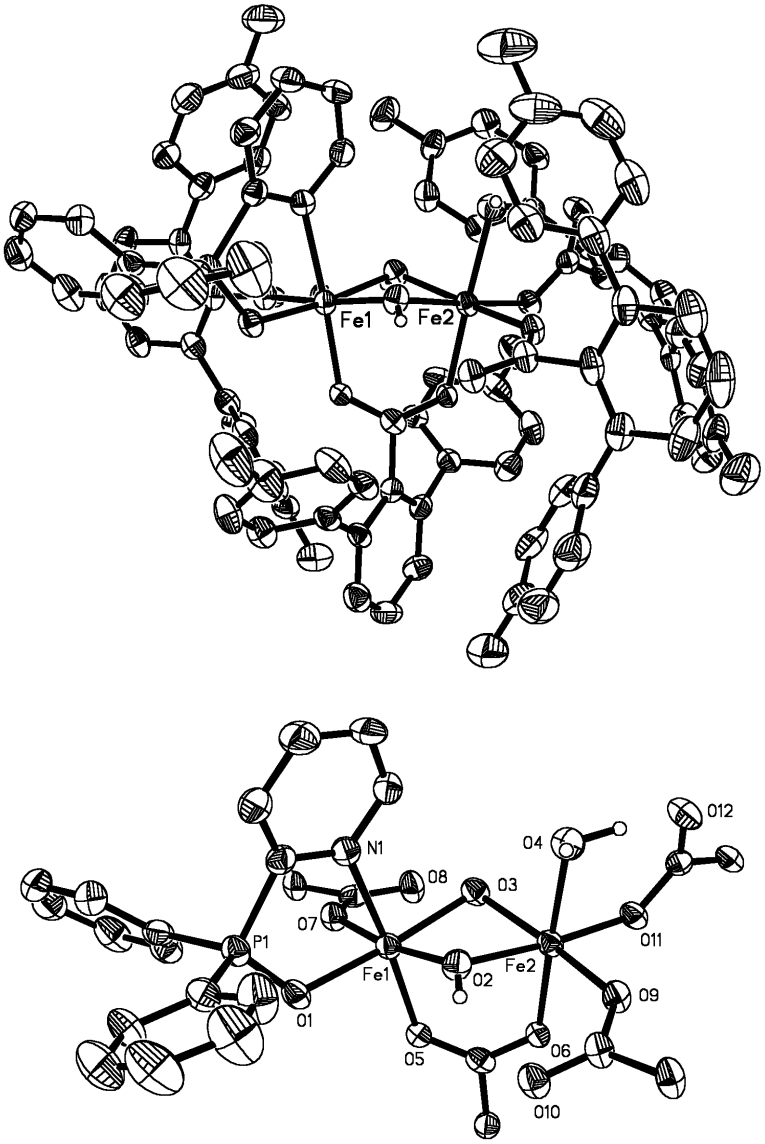

Figure S6. Carson and Lippard

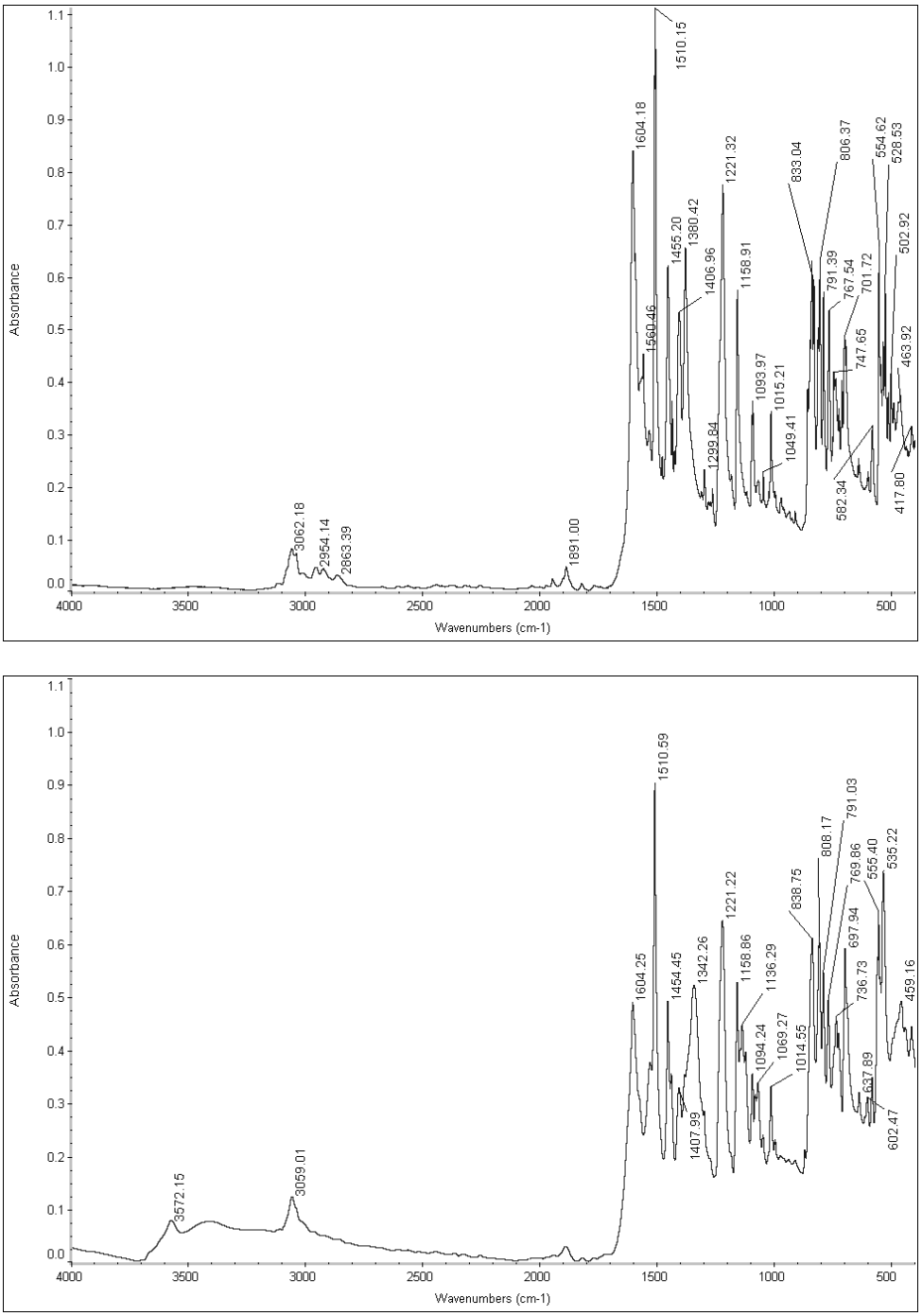

Figure S7. Carson and Lippard

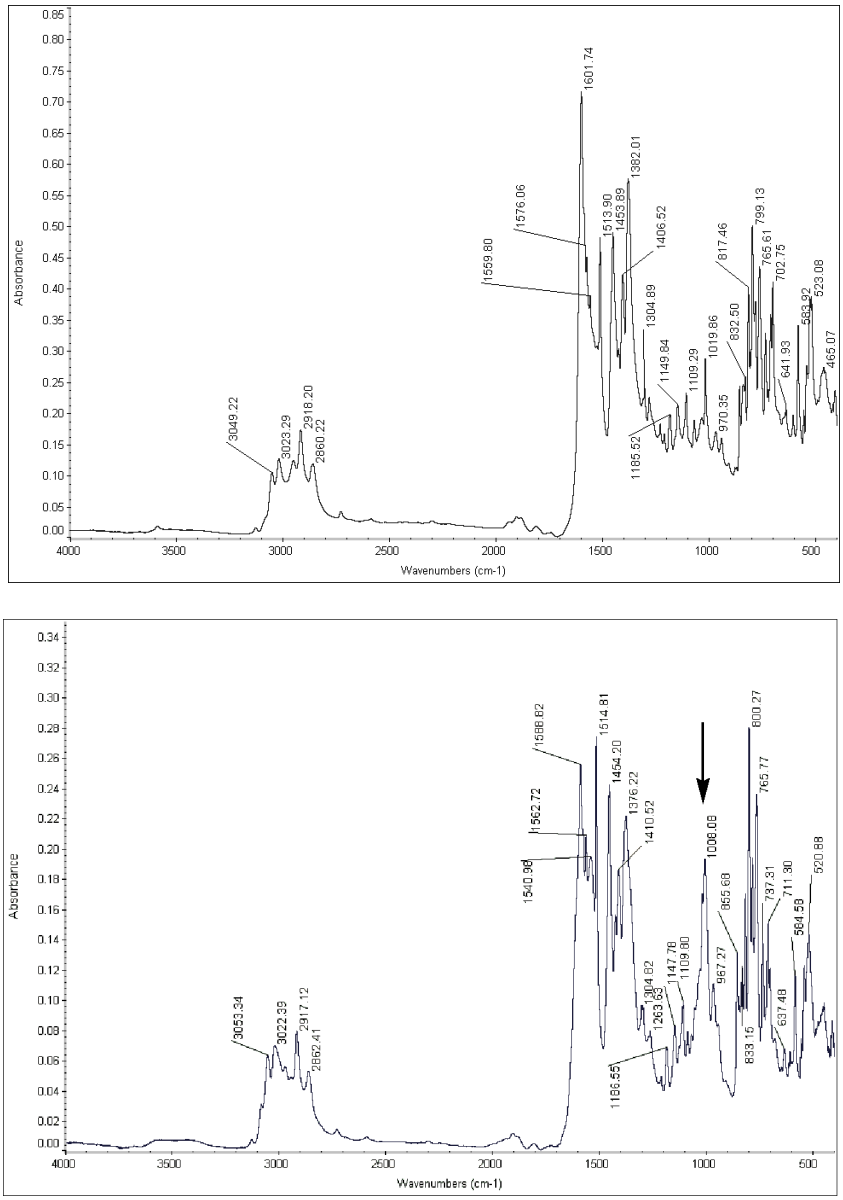

Figure S8. Carson and Lippard

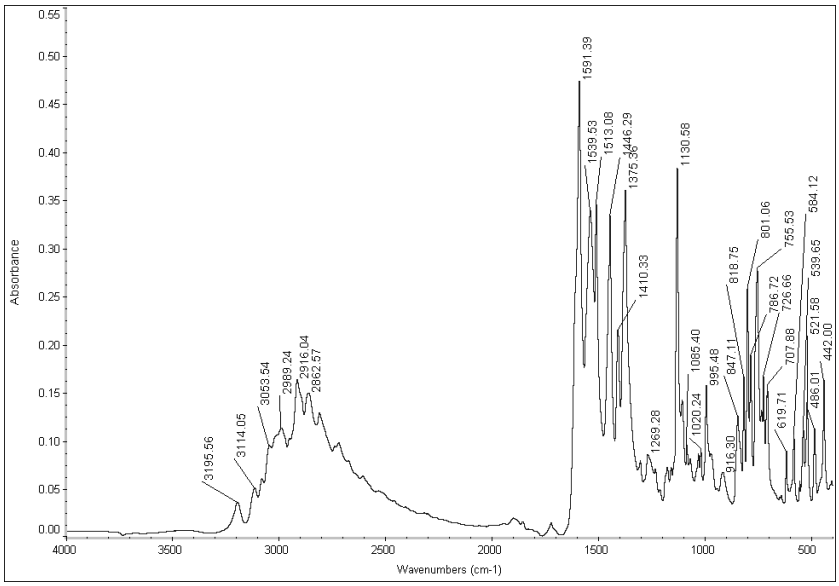

Figure S9. Carson and Lippard

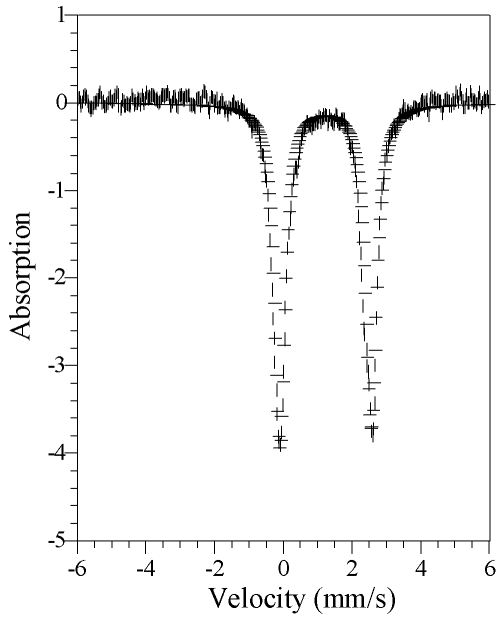

Figure S10. Carson and Lippard